

HyperSBINN: A Hypernetwork-Enhanced Systems Biology-Informed Neural Network for Efficient Drug Cardiosafety Assessment

Inass Soukarieh^{2,3}, Gerhard Hessler¹, Hervé Minoux²,
Marcel Mohr¹, Friedemann Schmidt¹, Jan Wenzel¹,
Pierre Barbillon³, Hugo Gangloff³, Pierre Gloaguen^{4,*}.

¹ Sanofi, R&D Preclinical Safety, Industriepark Hoechst,
Frankfurt am Main, Germany

² Sanofi, Digital R&D, 13 Quai Jules Guesde,
Vitry-Sur-Seine, France

³ Université Paris-Saclay, AgroParisTech, INRAE,
UMR MIA Paris-Saclay, 91120, Palaiseau, France.

⁴ Université Bretagne Sud, UMR CNRS 6205,
LMBA, F-56000 Vannes, France

*pierre.gloaguen@univ-ubs.fr;

August 27, 2024

Abstract

Mathematical modeling in systems toxicology enables a comprehensive understanding of the effects of pharmaceutical substances on cardiac health. However, the complexity of these models limits their widespread application in early drug discovery. In this paper, we introduce a novel approach to solving parameterized models of cardiac action potentials by combining meta-learning techniques with Systems Biology-Informed Neural Networks (SBINNs). The proposed method, HyperSBINN, effectively addresses the challenge of predicting the effects of various compounds at different concentrations on cardiac action potentials, outperforming traditional differential equation solvers in speed. Our model efficiently handles scenarios with limited data and complex parameterized differential equations. The HyperSBINN model demonstrates robust performance in predicting APD90 values, indicating its potential as a reliable tool for modeling cardiac electrophysiology and aiding in preclinical drug development. This framework represents an advancement in computational modeling, offering a scalable and efficient solution for simulating and understanding complex biological systems.

Keywords: System-Biology informed neural network, Hypernetwork and Cardiac action potential.

1 Introduction

The heart is one of the most important target organs of human drug toxicity. Consequently, modern drug discovery strives to screen out potential hazards early amongst multiple drug can-

didates, before an optimized drug candidate is selected and enters clinical trials. Toxicity testing has historically relied on evaluation of the adverse effects of drugs in dedicated animal studies to predict human safety of drug exposure. With the implementation of novel *in silico* predictive approaches, animal-free and cost-effective approaches are increasingly being developed to augment and ultimately replace animal experimentation (Jenkinson et al. (2020)). Amongst others, the cardiac action potential (CAP) (András et al. (2021)) is considered as a key parameter to monitor closely for undesired drug effects. CAP is a periodic and transient change of the membrane potential of heart cells. It is instantiated by a group of specialized pacemaker cells, which have automatic action potential generation capabilities. The voltage change is created by transport of charged ions through ion channels within the membrane. In healthy and undisturbed condition, the action potential passes along the cell membrane causing heart cells to contract periodically. Upon exposure to certain drugs, the morphology and frequency of the cardiac action potential can be disturbed, making this parameter an important marker for drug toxicity to the heart. CAP is tightly controlled by proper functioning of multiple ion channels expressed on cardiac myocytes. The ionic currents through channels maintain regular heart beat. Mathematical models of cardiac electrophysiology usually start from the modeling of ionic current dynamics in single cells, coupled with models for the propagation of an action potential in tissue, and ultimately also mechanical parameters, such as contractility, cardiac output or blood pressure. The general approach to cardiac electrophysiology applies a set of coupled differential equations (Trayanova et al. (2024); Mayourian et al. (2018)). Drugs may have the potential to alter the ion fluxes through undesired blocks of one or even multiple channels. These "off-target" effects have been found to be quite common, particularly with the human Ether-à-go-go-Related Gene (hERG) potassium channel(Lee et al. (2019)). Effects of drugs on ion channels can be mathematically expressed by partial block of the channels, leading to a reduced or stopped ionic current, and eventually implying alterations of the cardiac action potential(Gerlach (2001); Carmeliet and Mubagwa (1998); András et al. (2021)).

CAP modeling often employs systems of ordinary (ODEs) or partial differential equations (PDEs) such as the Hodgkin-Huxley equations or the Fitzhugh-Nagumo equations Corrias et al. (2011); Williams and Mirams (2015). However, these models can be computationally expensive, limiting their practical utility in the early drug development process where numerous drug candidates or even drug candidate libraries have to be assessed in parallel to guide drug development optimally. To address this challenge, we propose testing Physics-Informed Neural Networks (PINNs) as an innovative deep learning tool for solving CAP model (Raissi et al. (2019); Cuomo et al. (2022); Krishnapriyan et al. (2021))). PINNs combine the precision of governing physical laws with the efficiency of deep learning.

Classical PINNs solve differential equations by embedding physical laws into the neural network framework through a specialized loss function. This integration allows PINNs to leverage the strengths of machine learning, such as automatic differentiation and optimization, to solve complex scientific and engineering problems Raissi et al. (2019). A significant advancement in the application of PINNs is their use in handling stiff ODE systems, which are characterized by solutions that can change rapidly and require careful numerical treatment(Yazdani et al. (2020); Ji et al. (2021); O'Leary et al. (2022)). Traditional numerical methods for stiff ODEs, like implicit solvers, can be computationally expensive and challenging to implement. PINNs offer a promising alternative by directly incorporating the stiffness of the system into the training process, thus providing a more efficient and scalable solution.

Recent work has started to explore the use of PINNs to analyze cardiac electrophysiology models. For instance, Sahli Costabal et al. (2020) employed PINNs to solve the isotropic diffusion equation using *in silico* data, estimating action potential arrival times and conduction velocity maps. Grandits et al. (2021) advanced this work by solving the anisotropic eikonal equation

to learn about fiber orientations and conductivity tensors, though their study was based on synthetic data and data from only one patient. In a closely related study, Herrero Martin et al. (2022) applied PINNs with the monodomain equation to estimate electrophysiology parameters from sparse transmembrane potential maps, utilizing the Aliev-Panfilov model as described by Aliev and Panfilov (1996), which lacks biological mechanism. Most recently, Chiu et al. (2024) proposed a novel PINNs framework to predict how anti-arrhythmic drugs modulate myocardial electrophysiology parameters using in vitro optical mapping data and a biophysically detailed Fenton-Karma model.

Though algorithmic progress in machine learning is undisputed, the acquisition of suitable training data remains a challenge, leading to limited information available to inform models. Data-driven machine learning techniques, such as deep neural networks, tend to fail under these circumstances. Physics-Informed Machine Learning (PiML) addresses this by blending data-driven machine learning with physics-based simulations. This hybrid approach is transforming problem-solving in science, engineering, and medicine Alber et al. (2019). At the core of PiML are PINNs, a novel "meshfree" approach that leverages deep learning to solve PDEs commonly used to describe various phenomena in science and engineering. PINNs incorporate physical domain knowledge as soft constraints on an empirical loss function, optimized using existing machine learning training methodologies.

However, standard PINNs typically solve for a single set of parametrizations, meaning they are configured to solve the differential equations with specific fixed parameters. Therefore, when working in domains that require evaluating solutions across multiple parameter values, it is essential to adjust the approach to accommodate varying parameters. Two primary strategies for handling varying parametrizations in PINNs are prevalent:

1. Retraining the network: This involves training a new PINN for each distinct set of parametrizations, which is costly due to the time-intensive nature of training.
2. Including parameters as inputs: This approach increases the complexity of the PINN by directly propagating parametrizations into the network, resulting in decreased operational speed.

To solve this problem, this study introduces the use of HyperPINN in conjunction with a highly validated mathematical CAP model presented by Mohr et al. (2022). HyperPINN, developed by de Avila Belbute-Peres et al. (2021), adopts a meta-learning approach, utilizing a separate network (hypernetwork) to understand how parameters influence the equation. This allows the primary network responsible for solving the equation to remain simple and efficient.

In our specific case, the parametrization variables of the ODE systems pertain to the compound's half-maximal inhibitory concentration (IC50) for a selection of four ionic channels: hERG potassium channel, hKv4.3 potassium channel, hCav1.2 L-type calcium channel, and hNav1.5 sodium channel. Each set of these four parameters characterizes the inhibitory potency of an individual compound on these selected channels. Given our objective of testing multiple compounds simultaneously, we encounter challenges in parametrized physics-informed neural networks, such as solving complex differential equations with a high number of parameters, handling high-dimensional parameters space, and ensuring accurate predictions across various parameter combinations.

This paper presents results utilizing HyperPINN, referred to as HyperSBINN, integrating hypernetworks and system biology-informed neural networks (SBINNs). Our approach highlights the significance and effectiveness of employing hypernetworks to train the parameter space of IC50 values. We compare our findings with other machine learning techniques, to demonstrate the efficacy of HyperSBINN.

2 Cardiac action potential model

Our study focuses on the modelling of the cardiac action potential (CAP) under different drug configurations. We focus on the model proposed by Mohr et al. (2022), which we briefly recall here.

In our context, the effect of a drug on CAP is supposed to depend only on its concentration (denoted D) and on the inhibitory effect of the drug on J ionic channels. The inhibitory effect of the j -th ($1 \leq j \leq J$) ionic channel is denoted by $IC50_j$. We denote $\mathbf{X} = \{D, IC50_1, \dots, IC50_J\}$ the controlled characteristics of the drug. The CAP $V(t, \mathbf{X})$ at time t under the configuration \mathbf{X} is related to $J = 8$ ionic currents (listed in the Appendix A), denoted by $I_j(t, \mathbf{X})$ ($1 \leq j \leq 8$) through the ordinary differential equation (ODE)¹

$$\frac{dV}{dt}(t, \mathbf{X}) = - \left(I_{\text{stim}}(t) + \sum_{j=1}^8 I_j(t, \mathbf{X}) \right), \quad (1)$$

where $I_{\text{stim}}(t)$ is a known externally applied stimulus current (see Appendix). The generic formulation of an ionic current $I_j(t, \mathbf{X})$ from a channel j is based on Ohm's law and can be stated as

$$I_j(t, \mathbf{X}) = G_j \cdot k_j(D, IC50_j) \cdot g_j(t, V(t, \mathbf{X})) \cdot (V(t, \mathbf{X}) - E_j), \quad (2)$$

where:

- E_j and G_j is the known reversal potential and the maximal conductance, respectively, for channel j ;
- $k_j(D, IC50_j)$ is a function describing the inhibition factor for channel j . This function is either always 1 (no inhibition), or takes the following form for the four ionic channels listed in the Appendix:

$$k_j(D, IC50_j) = \left(1 + \frac{D}{IC50_j} \right)^{-1}.$$

- $g_j(t, V(t, \mathbf{X}))$ is the fraction of conducting channels, which depends on voltage and a set of kinetic parameters. It depends on $V(t, \mathbf{X})$ through ODEs (resulting in 13 ODEs, all listed in the Appendix A).

The complexity of the proposed models lies in the expressions of $V(t, \mathbf{X})$ and the different $g_j(t, V(t, \mathbf{X}))$, which requires solving a (nonlinear) system of 14 ODEs, whose solution has a nonlinear dependence on \mathbf{X} , to obtain a CAP curve for each drug configuration. We denote by $u(t, \mathbf{X})$ the function taking values in \mathbb{R}^{14} which is the solution of our system of ODE. The next section depicts the framework to obtain a fast approximation of this function for every t and \mathbf{X} without using an ODE solver for each configuration \mathbf{X} .

3 System Biology-Informed Neural networks

3.1 Overview of Physics-Informed Neural Networks

In this first part, we focus on the approximation of the solution for a given \mathbf{X} . Thus this variable is omitted in the notation. Consider the problem of approximating a function $u(t) \in \mathbb{R}^d$, for

¹This is the classical equation for electrical properties of a single cardiac cell, where we set the cell capacitance to 1, as in Mohr et al. (2022).

$t \in [0, T]$ (where T is a fixed time horizon), such that $u(t)$ is the solution of a nonlinear system of differential equations, expressed as:

$$\begin{aligned} u(0) &= \mathbf{u}_0 \\ \frac{du}{dt}(t) &= f(u(t)), \end{aligned} \quad (3)$$

where $f(\cdot)$ is a known non linear function and \mathbf{u}_0 is the known initial condition. We suppose moreover that we have a set of measurements $y_{1:n} := y_1, \dots, y_n$ from the target function² at times $t_{1:n} := t_1, \dots, t_n$.

Physics-informed neural networks (PINNs, Raissi et al., 2019), approximates the solution u by a function $v(t, \theta)$, which is a neural network parameterized by a set of weights and biases θ . Neural networks provide a flexible set of arbitrarily complex functions that performs well in approximating non linear functions and whose derivatives (with respect to t or θ) can be easily computed by automatic differentiation in standard machine learning softwares. For a given neural network architecture³, the approximation problem boils down to learn θ that minimize some loss function $\mathcal{L}(\theta)$. In our context, a "good" approximation is a function $v(t, \theta)$ such that:

- at observation times t_1, \dots, t_n , the observations are well approximated, *i.e.*, for all $1 \leq i \leq n$, $v(t_i, \theta) \approx y_i$.
- the approximation satisfies the initial condition, *i.e.* $v(0, \theta) \approx \mathbf{u}_0$.
- the approximation satisfies Equation (3), *i.e.*, for all $t \in [0, T]$,

$$\frac{dv}{dt}(t, \theta) \approx f(v(t, \theta)).$$

These three objectives result in the following loss for the PINN:

$$\mathcal{L}^{\text{PINN}}(\theta) = w^{\text{Data}} \mathcal{L}^{\text{Data}}(\theta) + w^{\text{IC}} \mathcal{L}^{\text{IC}}(\theta) + w^{\text{ODE}} \mathcal{L}^{\text{ODE}}(\theta), \quad (4)$$

where w^{Data} , w^{IC} and w^{ODE} are weights chosen by the user and:

$$\begin{aligned} \mathcal{L}^{\text{Data}}(\theta) &= \frac{1}{n} \sum_{i=1}^n \|v(t_i, \theta) - y_i\|^2, && \text{Data loss} \\ \mathcal{L}^{\text{IC}}(\theta) &= \|v(0, \theta) - \mathbf{u}_0\|^2, && \text{Initial condition loss} \\ \mathcal{L}^{\text{ODE}}(\theta) &= \frac{1}{m} \sum_{j=1}^m \left\| \frac{dv}{dt}(\tau_j, \theta) - f(v(\tau_j, \theta)) \right\|^2. && \text{ODE loss} \end{aligned}$$

The first two losses are mean squared errors at the observed values of the function. The third loss, evaluates the adequacy of the derivative of the approximation to the ODE model, at times τ_1, \dots, τ_m that are chosen by the user. These times are the analogous of the discretization times in a scheme use by a traditional ODE solver.

By optimizing θ (typically using gradient descent), one can therefore find a model that both fits the data and satisfies the physics equation. However, so far, the training of θ must be done separately for each drug configuration \mathbf{X} . We now depict a unified framework for all drug configurations.

Note that the choice of the weights w^{Data} , w^{IC} and w^{ODE} will affect the training. This choice is model-driven and is discussed for our case study in Section 5.2. Note that we wrote Equation (3) with a common weight for all ODEs, but it is straightforward to have different weights for the different ODEs (which turned out to be necessary in our case-study).

²Still, in this section, observations would come from a single drug configuration \mathbf{X} .

³Defined by the number of layers, the number of neurons per layers, the connections between layers, and the activation functions.

3.2 HyperPINN

We now come back to our original objective which is to learn the function $u(t, \mathbf{X})$ given by the CAP model of Section 2, for the drug configuration \mathbf{X} .

Once a good PINN architecture has been chosen a natural approach would be to learn a mapping which, for a configuration \mathbf{X} , gives the parameters $\theta(\mathbf{X})$ for which $v(t, \theta(\mathbf{X}))$ is a good approximation of $u(t, \theta)$. This approach, named hyperPINNs, was introduced by de Avila Belbute-Peres et al. (2021). It combines physics-informed neural network architectures with hypernetworks (Ha et al., 2016). The main idea is then to build a neural network $v_{\text{hyper}}(x, \Gamma)$, parameterized by Γ , that takes as input a drug configuration and outputs a parameter θ which serves at the weights for a neural network $v_{\text{PINN}}(t, \cdot)$. Formally, we approximate $u(t, \mathbf{X})$ by setting, for every $(t, \mathbf{X}) \in [0, T] \times \mathbb{R}^5$:

$$\begin{aligned} \theta(\mathbf{X}) &:= v_{\text{hyper}}(\mathbf{X}, \Gamma) , \\ \hat{u}(t, \mathbf{X}) &:= v_{\text{PINN}}(t, \theta(\mathbf{X})) . \end{aligned}$$

The learning objective then becomes to optimize the loss in Γ . Supposed that we have at disposal a set of q drug configurations $\mathbf{X}_1, \dots, \mathbf{X}_q$, and that for each configuration, we have a specific set of observations and times for the ODE loss (defined in Section 3.1). The loss for the hyperPINN then becomes:

$$\mathcal{L}^{\text{hyperPINN}}(\Gamma) = \sum_{i=1}^q \mathcal{L}^{\text{PINN}}(v_{\text{hyper}}(\mathbf{X}_i, \Gamma)) .$$

where $\mathcal{L}^{\text{PINN}}$ is defined in Equation (4). Figure 1 depicts graphically the framework of hyperPINNs.

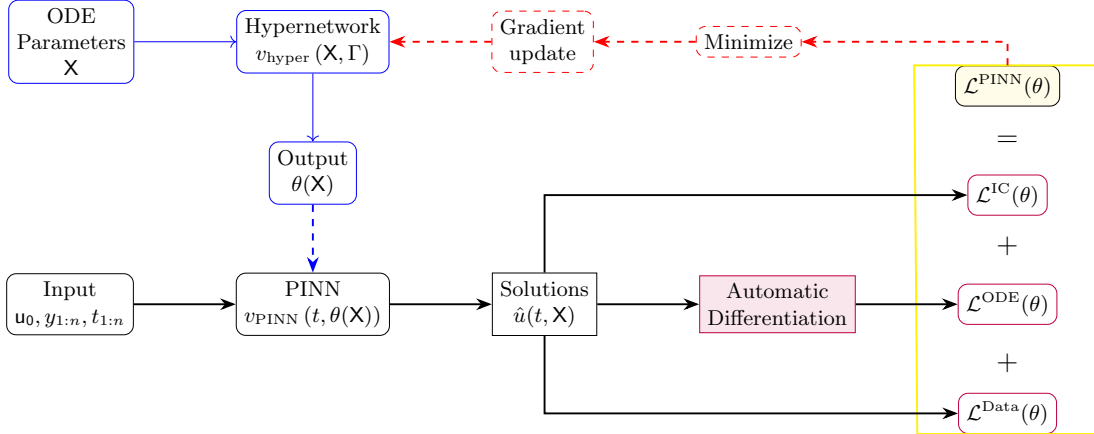


Figure 1: The two-stage neural network architecture of HyperPINNs. The hypernetwork takes a set of configuration \mathbf{X} as input and outputs the weights and biases for the main PINNs network. The PINNs network then takes a time coordinate as input and makes predictions based on the problem defined by the hypernetwork output.

4 Experimental settings

In our approach, called HyperSBINN, we combine systems biology-informed neural networks, defined in Yazdani et al. (2020), with hypernetworks to predict CAP at various concentrations.

Our input X is a vector of size 5, stacking the IC50 values of four cardiac ion channel targets of interest (hERG, hKv3.4, hCav1.2, and hNav1.5), and the drug concentration. The model then outputs 14 curves, and in particular the curve of $V(t)$, which is our main target.

We assess the performance of our approach by first comparing the curves outputted by the HyperSBINN to the curves outputted by the solver and second, by computing a quantity of interest (biomarker) from the voltage curve, namely APD90. Since this quantity of interest is scalar, we can compare our HyperSBINN approach with standard machine learning techniques.

4.1 Assessing performance of the hyperSBINN model

We assess the performance of the hyperSBINN model to retrieve the solution of the ODE system for different set of drug configurations when the train is performed using our different losses. As observations, we provide outputs of a SBINN solver at random times (uniformly in $[0, 500\text{ms}]$) for random drug configurations. We uniformly randomly generated a total of 500 different drug configurations. These configurations include uniformly simulated IC50 values for four ionic channels, ranging from $0.1 \mu\text{M}$ to $100 \mu\text{M}$, and drug concentrations D varying between $0 \mu\text{M}$ and $4 \mu\text{M}$.

4.2 Learning specific biomarker of the CAP

As mentioned previously, the curve $V(t)$ is the target output. From this curve, we can extract significant biomarker responses such as the APD50, the peak value, and others. An important biomarker is the APD90 response, which is defined as the time it takes for the membrane potential to repolarize to 90% of its peak value during an action potential. Mathematically, it can be expressed as:

$$\text{APD90} = t_{90} - t_{peak},$$

where t_{90} is the time at which the membrane potential $V(t)$ repolarizes to 90% of its peak value, and t_{peak} is the time at which $V(t)$ reaches its peak value. These values are obtained directly from the $V(t)$ curves. To evaluate the effectiveness of the HyperSBINN model, we will compare its predictions of APD90 values across a set of the same drug configurations as in the previous part. The HyperSBINN model was used to predict the voltage curves $V(t)$, from which the APD90 values were subsequently extracted. The absolute difference with the numerical solver (considered as the ground truth) is then computed for each configuration in the test set. Additionally, we will compare the APD90 predicted by the HyperSBINN with those obtained from a Random Forest model, a standard machine learning technique which has provided the best performances in this case. While the methodologies differ, the comparison aims to evaluate performance of predicting the APD90. The Random Forest model will be trained using the same configuration set as the hyperSBINN (see Section 2), and will predict APD90 values directly, bypassing the voltage curve $V(t)$ and the CAP model.

5 Implementation details

In this section, we provide details of our implementation HyperSBINN. Python (3.10) was used for all numeric computations. HyperSBINN model was designed, trained and deployed using the Python library `Jinns`⁴. Note that the training of the HyperSBINN is time demanding, its evaluation (once trained) is fast.

⁴<https://github.com/mia-jinns/jinns>

5.1 HyperSBINN architecture and training

For the SBINN, a Multi-Layer Perceptron (MLP) architecture with one input the time space t , five hidden layers with 50 neurons each, and an output layer of size 14. The hypernetwork is also a MLP with input of size 5, and five hidden layers of 46 neurons. The output size corresponds to the required number of parameters for the SBINN network. The choice of these architectures was guided by different experimentations, where we tested different combinations to find the optimal configuration that balances computational efficiency and model performance. The specific architecture was selected based on its ability to capture the complexity of the CAP model while maintaining manageable computational costs.

Regarding the activation function, we use the hyperbolic tangent activation function for all layers except the last one. The output layer matches the possible values taken by the solutions of the ODEs, which is $[0, 1]$ for the 13 gate functions and $]-\infty; +\infty[$ for the voltage function. The match is made by using sigmoid and linear activation functions respectively. For the hypernetwork, we consistently use the hyperbolic tangent activation function.

For stochastic gradient descent, we used the Adamax optimizer (Kingma and Ba, 2014), a variant of the Adam optimizer, with a learning rate being constant at 10^{-4} for 10,000 iterations, then decreasing linearly to 10^{-6} until iteration 50000, and being constant to this value for remaining iterations. This optimizer was chosen due to its suitability for problems with potentially very large gradients, which can be common in deep learning tasks. Unlike Adam, which uses an exponentially decaying average of squared gradients, Adamax utilizes the infinity norm (maximum absolute value) of past gradients. In our case, this optimizer was essential as it effectively handled gradients that fluctuate significantly, leading to more stable and efficient learning in our model.

5.2 Losses weights

The weights discussed in Section 3.1 were meticulously selected to ensure balanced contributions from all terms in the loss function. The weights w^{ODE} were chosen so that all terms in the ODE loss function contribute at a similar scale, preventing any single ODE from dominating the optimization process and ensuring the model learns from all aspects of this loss function. The detailed method used for selecting these weights is provided in Appendix B.

The weight w^{IC} for the initial condition loss term was set to 1 to prioritize satisfying the initial points during training, ensuring the model adheres to the starting state of the system. Additionally, the weights for the observational data loss w^{Data} were also set to 1. This configuration allows the model to learn from the physical dynamics and governing ODEs while still incorporating observations, but without giving them undue influence over the training process.

5.3 Collocation points

To avoid overfitting to specific collocation points, the ODE loss is computed with batches of 500 times (in $[0, 500]$) which were uniformly sampled at each iteration. This sampling strategy certainly avoids overfitting, but could be improved by sampling in times zones where the model performs poorly.

For readers who want to reproduce our study, it is worth noting that a preprocessing step is necessary to ensure efficient neural network training. We address this by employing a linear scaling mechanism for the time variable t . This involves normalization by dividing t by the maximum time domain value, T_{max} . This transformation $t = t/T_{max}$ compresses the t scale to a more manageable range, typically around $O(1)$, for optimal NN performance.

5.4 Observational Data points

As we stated in Section 4, we will add some observational data ($y_{1:n}$) to the network. We derive these observations by extracting configurations X from the hypernetwork, and then we used a numerical solver to generate the solution of the CAP model given these configurations. For the numerical solver, we use the same initial conditions provided to the HyperSBINN model and described above.

Generated data are provided to the network as an input and used to minimise the data discrepancy loss function, and introduced in the loss function l_{Data} in Equation (4). From the extensive dataset, we randomly select 0.6 % data points of the total generated data, injecting them into the hyperSBINN along with their corresponding time and configuration X . This augmentation strategy enhances the robustness and generalization capabilities of our network architecture.

6 Results

6.1 Performance of the hyperSBINN model

This section presents a series of experimental results. Figure 2 presents the convergence behavior of the loss components described in Section 3.1 during the training of the HyperSBINN model. The graph demonstrates the training dynamics of the HyperSBINN, with a significant initial drop in the dynamic loss (\mathcal{L}^{ODE}) indicating rapid learning of the underlying ODEs. The steady decrease and eventual stabilization of the initial condition loss and observation loss suggest effective learning of initial conditions and a good fit to the observed data. One can notice high variability of the ODE loss, which makes the learning highly sensitive to the learning rate schedule. The training of the HyperSBINN takes around two hours but once it is trained, an evaluation takes only a few seconds which is twenty times faster than using the ODE solver.

The results from the HyperSBINN model presented in 3 closely match those obtained from the numerical solver across all variables, with minor differences observed in transition phases. This close alignment indicates that the HyperSBINN effectively captures the system’s dynamics and provides comparable performance to the traditional solver. The slight discrepancies in signal with low range of variations (such as h_{K-S} , h_{Ca-L} or h_{To-S} might be corrected by adjustment of the different ODE weights.

Figure 3 also presents a comparative analysis between the traditional solver and the HyperSBINN model for two sets of parameterizations over a time span of 500 milliseconds. The HyperSBINN model demonstrates high accuracy in replicating the results from the traditional solver across all variables. This can be seen in Table 1 which provides the normalized squared differences between curves outputted by the numerical solver and curves provided by the HyperSBINN on a test set of drug configurations. The order of magnitude is low for a vast majority of configurations. However, a few configurations (two over 500 in our test set) present a strong discrepancy.

We have noticed the importance of observed data, as the training without the observation loss would lead, in most of the time to solution which are constant outside of the initial conditions (not shown here). Therefore, to ensure the model captures the full range of possible solutions, it is crucial to incorporate additional data points that represent the solutions of the ODE system at different time points t , beyond just the initial conditions and ODE loss.

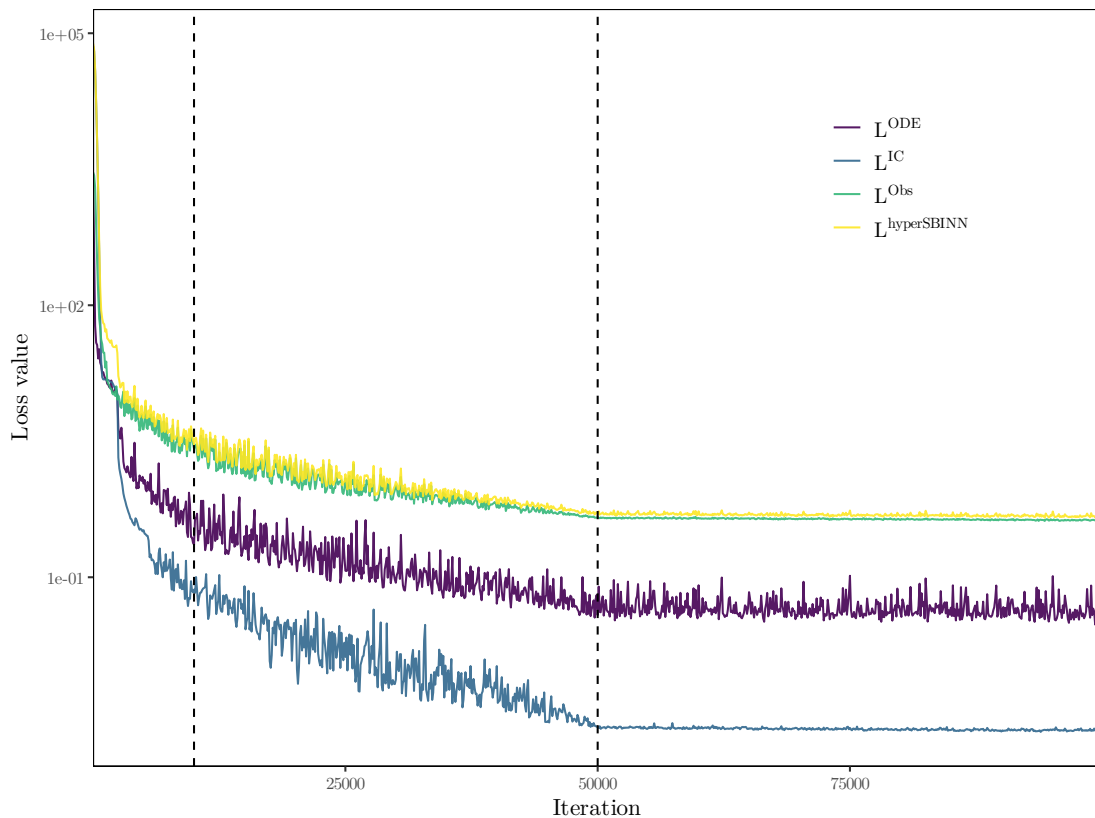


Figure 2: Convergence behavior of different loss components (in log scale) during the training of HyperSBINN. To ease the read, loss values have been smoothed using a moving average over 500 iterations. The learning is constant and equal to 10^{-4} until iteration 10000 (first dashed line), then decreases linearly to 10^{-6} (second dashed line), and remains constant afterwards.

6.2 Learning specific biomarker of the CAP

Table 2 shows the absolute error of prediction of APD90 when this quantity is computed using the voltage curve output by the hyperSBINN. Overall, the prediction is satisfying, as the discrepancy between target and prediction is less than 3 ms for 75% of predictions.

It is worth noting that if the specific goal is the prediction of this quantity, and if the user has a training set of APD90s for different drug configurations, a classical machine learning algorithm (that focuses on this specific quantity) might be a better option. For instance, Table 2 illustrates that a dedicated random forest performs quite well for this task. This is not a surprise as a perfect prediction of the APD90 from the voltage curves requires a perfect approximation of the lowest value, the highest value, and the decreasing rate. A small error on those three quantities could accumulate when predicting the APD90. Moreover, as shown before, the hyperSBINN model is susceptible to extreme values in the error. Having a specific sampling design for problematic drug configurations (instead of the uniform sampling chosen here) is certainly a lead for future work.

Curve	Min	Q1	Median	Mean	Q3	Max
$V(t)$	0.01	0.07	0.16	1.71	0.59	161.49
f_{Ca-L}	0.02	0.05	0.10	1.21	0.42	173.76
h_{Ca-L}	0.08	0.23	0.54	2.36	1.41	178.18
f_{Na-F}	0.19	0.27	0.46	4.61	1.61	436.78
f_{Na-L}	0.12	0.30	0.42	0.99	0.72	43.92
h_{Na-f}	0.00	0.03	0.10	1.46	0.55	163.84
h_{Na-L}	0.01	0.03	0.08	1.26	0.40	185.51
f_{To-F}	0.03	0.05	0.10	1.04	0.30	228.93
f_{To-S}	0.07	0.11	0.15	1.25	0.35	250.48
h_{To-F}	0.11	0.16	0.20	1.24	0.41	185.34
h_{To-S}	7.40	13.36	14.67	17.33	16.83	219.86
f_{K-R}	0.04	0.09	0.15	1.40	0.40	183.74
f_{K-S}	0.10	0.23	0.47	1.83	1.17	193.82
h_{K-S}	0.92	1.55	1.84	3.37	2.97	144.10

Table 1: Normalized squared differences between curves outputted by the solver and curves outputted by the SBINN. All metrics were multiplied by 1000, for instance, a value of 200 corresponds to a normalized squared difference of 0.2.

Method	Min	Q1	Median	Mean	Q3	Max
hyperSBINN	0.000	0.600	1.300	2.972	2.900	90.800
RF	0.000	0.071	0.189	0.627	0.454	25.613

Table 2: Absolute difference (in ms) between predicted and APD90 obtained by the python solver. Predictions are made over 500 drug configurations.

7 Conclusion and perspectives

In this work, we introduce a new framework for modeling cardiac electrophysiology using System Biology-Informed Neural Networks (SBINNs) enhanced with hypernetworks. This approach addresses the limitations of traditional SBINNs by incorporating hypernetworks for parameterized differential equations, providing a more robust and scalable model of cardiac action potentials. Our HyperSBINN approach successfully integrates systems biology-informed neural networks with the flexibility and efficiency of hypernetworks, enabling the simultaneous prediction of cardiac action potentials across drugs at variable concentrations.

The complexity of our HyperSBINN model stems from various factors. The system involves numerous interacting equations, making the training process longer and more resource-intensive. Additionally, the model features a high number of non-fixed parameters (5 parameters that represent the drug configuration X) with a large range of the IC50 values ($[0.1 - 100]$). This significantly expands the search space, requiring the optimizer to explore extensively to find the optimal solution, potentially leading to slow training times. The numerous factors mentioned above contribute to a slower optimization process. The optimizer might take a long time to find a good solution or risk getting stuck in local minima. With a complex differential equation system and many parameters, there is a higher risk of the model overfitting to the training data. This means the model might perform well on the training data but fail to generalize to unseen data. The hyperparameters of the neural network become even more crucial for successful training. Careful tuning is necessary to balance exploration and exploitation during optimization.

The results indicate that our model might achieve high accuracy in replicating results from

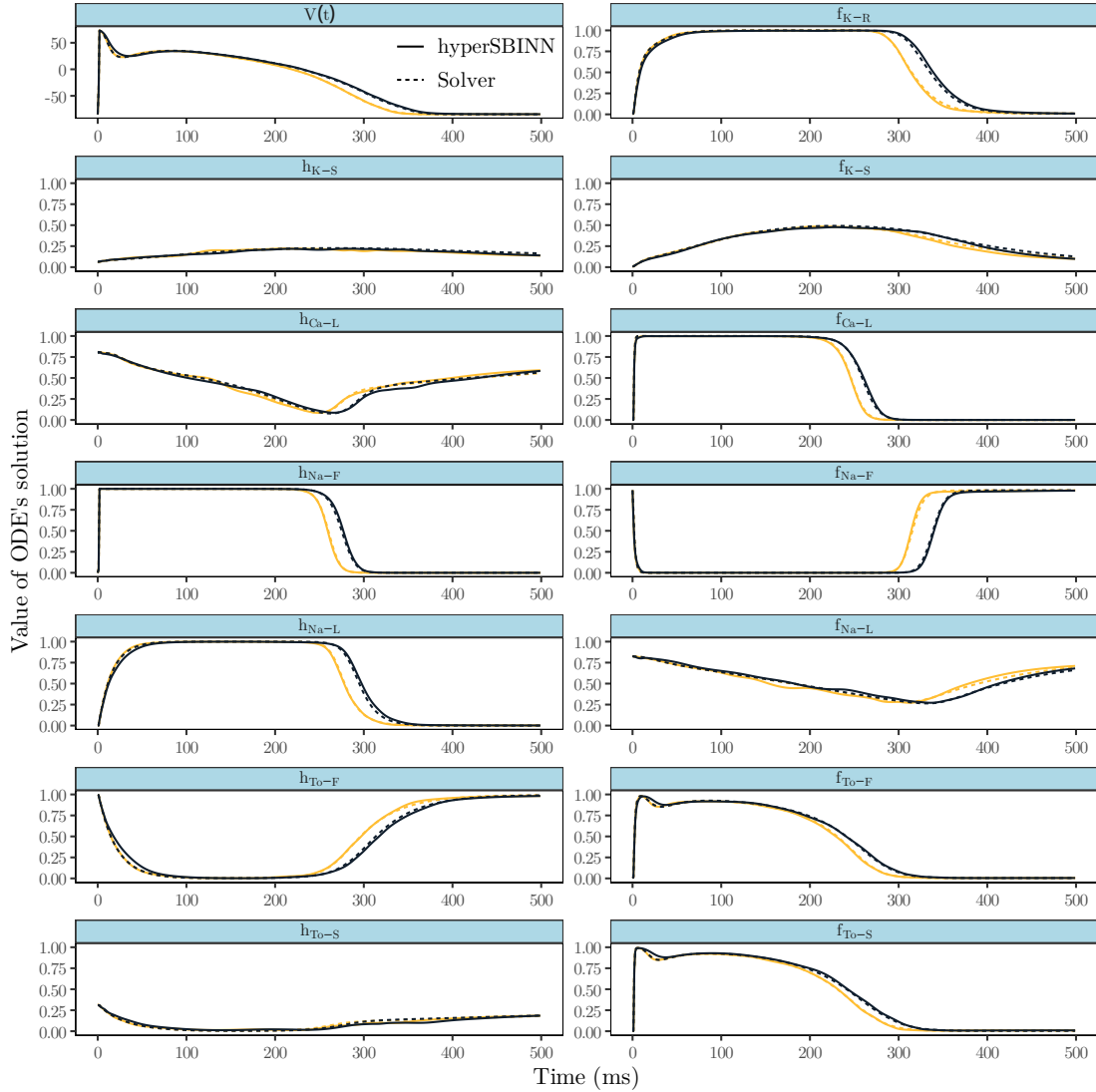


Figure 3: Comparison of the solver and hyperPINN curves for 2 different drug configurations never seen on the training set (one color per configuration) for each 14 solutions of the biological system. Significance of all signals names is depicted in Appendix. Our main signal of interest is $V(t)$ (top left).

traditional solvers. This close alignment underscores the model’s capability to effectively capture the dynamics of complex systems. Furthermore, the HyperSBINN model demonstrated robust performance in predicting APD90 values, showing comparable accuracy to a well-tuned Random Forest model.

In our work, we leverage Data-driving learning alongside the HyperSBINN model for several key reasons. First, incorporating observations, even a small portion, significantly improves the accuracy and convergence, especially when dealing with 1024 different curve solutions during the

training. This is particularly beneficial for complex systems of Ordinary Differential Equations (ODEs) where the model can encounter challenges identifying the correct solution manifold from scratch. Also, these observations act as guideposts, steering the HyperSBINN towards the physically relevant solutions within the vast solution space. Compared to literature findings where 10% to 20% of data might be used for a single curve solution, our approach shows remarkable efficiency. We achieve comparable accuracy using only 0.6% of the total observations data points for 1024 drugs configurations used for training. This is possible due to the model’s ability to learn from limited data and generalize across different configurations. This efficiency is particularly important when data acquisition is expensive.

To the best of our knowledge, this is the first instance where a systems biology-informed neural network is combined with a hypernetwork for the study of cardiac action potentials. Looking forward, further refinement and validation of the HyperSBINN model on more specific and diverse datasets are necessary to fully realize its potential. Expanding the framework with real clinical and *in vitro* data will be crucial for translating the model advancements into pharmaceutical applications. Additionally, improving the selection of observational data (explained in Section 5.4), ensuring that data points are more precise and representative, will enhance the model accuracy. For instance, incorporating more targeted observations at critical time points or under specific conditions could provide better guidance for the model. Furthermore, in our study, we compared our results with the solutions of the ODEs derived from a numerical solver. It would be interesting to also compare these results with real cardiac voltage curves and ionic currents derived from biological assays. Including real observation data for the gates and voltages would also be beneficial. Given that real data often contains noise, methodologies such as those proposed in the work Linka et al. (2022). Additionally, it can be interesting to adaptively manage collocation points based on model residuals, which could enhance the efficiency and accuracy of the training process as inNguyen et al. (2023).

Overall, the framework proposed in this work represents a promising step toward more efficient and reliable computational AI models in cardiac electrophysiology, potentially accelerating the development of safer and more effective drugs.

Acknowledgement

We thank H. Matter and C. Grebner for thoughtful discussions at the beginning of this project.

Author Disclosure Statement

G.H., H.M., M.M., F.S. and J.W. are employees of Sanofi and may hold shares in the company.

Funding Information

This research was supported by Sanofi.

References

Alber, M., Buganza Tepole, A., Cannon, W. R., De, S., Dura-Bernal, S., Garikipati, K., Karniadakis, G., Lytton, W. W., Perdikaris, P., Petzold, L., et al. Integrating machine learning and multiscale modeling—perspectives, challenges, and opportunities in the biological, biomedical, and behavioral sciences. *NPJ digital medicine*, 2(1):115, 2019.

- Aliev, R. R. and Panfilov, A. V. A simple two-variable model of cardiac excitation. *Chaos, Solitons & Fractals*, 7(3):293–301, 1996.
- András, V., Tomek, J., Nagy, N., Virág, L., Passini, E., Rodriguez, B., and Baczkó, I. Cardiac transmembrane ion channels and action potentials: cellular physiology and arrhythmogenic behavior. *Physiological reviews*, 2021.
- Carmeliet, E. and Mubagwa, K. Antiarrhythmic drugs and cardiac ion channels: mechanisms of action. *Progress in biophysics and molecular biology*, 70(1):1–72, 1998.
- Chiu, C.-E., Pinto, A. L., Chowdhury, R. A., Christensen, K., and Varela, M. Characterisation of anti-arrhythmic drug effects on cardiac electrophysiology using physics-informed neural networks. *arXiv preprint arXiv:2403.08439*, 2024.
- Corrias, A., Giles, W., and Rodriguez, B. Ionic mechanisms of electrophysiological properties and repolarization abnormalities in rabbit purkinje fibers. *American Journal of Physiology-Heart and Circulatory Physiology*, 300(5):H1806–H1813, 2011.
- Cuomo, S., Di Cola, V., Giampaolo, F., and Rozza, G. Scientific machine learning through physics-informed neural networks: Where we are and what’s next. *Journal of Scientific Computing*, 92:1–27, 2022.
- de Avila Belbute-Peres, F., Chen, Y.-f., and Sha, F. Hyperpinn: Learning parameterized differential equations with physics-informed hypernetworks. In *The symbiosis of deep learning and differential equations*, 2021.
- Gerlach, U. channel blockers: potential antiarrhythmic agents. *Drugs of the Future*, 26(5):473–484, 2001.
- Grandits, T., Pezzuto, S., Costabal, F. S., Perdikaris, P., Pock, T., Plank, G., and Krause, R. Learning atrial fiber orientations and conductivity tensors from intracardiac maps using physics-informed neural networks. In *International Conference on Functional Imaging and Modeling of the Heart*, pages 650–658. Springer, 2021.
- Ha, D., Dai, A., and Le, Q. V. Hypernetworks. *arXiv preprint arXiv:1609.09106*, 2016.
- Herrero Martin, C., Oved, A., Chowdhury, R. A., Ullmann, E., Peters, N. S., Bharath, A. A., and Varela, M. Ep-pinns: Cardiac electrophysiology characterisation using physics-informed neural networks. *Frontiers in Cardiovascular Medicine*, 8:768419, 2022.
- Jenkinson, S., Schmidt, F., Ribeiro, L. R., Delaunois, A., and Valentin, J.-P. A practical guide to secondary pharmacology in drug discovery. *Journal of Pharmacological and Toxicological Methods*, 105:106869, 2020.
- Ji, W., Qiu, W., Shi, Z., Pan, S., and Deng, S. Stiff-pinn: Physics-informed neural network for stiff chemical kinetics. *The Journal of Physical Chemistry A*, 125(36):8098–8106, 2021.
- Kingma, D. P. and Ba, J. Adam: A method for stochastic optimization. *arXiv preprint arXiv:1412.6980*, 2014.
- Krishnapriyan, A., Gholami, A., Zhe, S., et al. Characterizing possible failure modes in physics-informed neural networks. In *NeurIPS*, 2021.

- Lee, H.-M., Yu, M.-S., Kazmi, S. R., Oh, S. Y., Rhee, K.-H., Bae, M.-A., Lee, B. H., Shin, D.-S., Oh, K.-S., Ceong, H., et al. Computational determination of hERG-related cardiotoxicity of drug candidates. *BMC bioinformatics*, 20:67–73, 2019.
- Linka, K., Schäfer, A., Meng, X., Zou, Z., Karniadakis, G. E., and Kuhl, E. Bayesian physics informed neural networks for real-world nonlinear dynamical systems. *Computer Methods in Applied Mechanics and Engineering*, 402:115346, 2022.
- Mayourian, J., Sobie, E. A., and Costa, K. D. An introduction to computational modeling of cardiac electrophysiology and arrhythmogenicity. *Experimental Models of Cardiovascular Diseases: Methods and Protocols*, pages 17–35, 2018.
- Mohr, M., Chambard, J.-M., Ballet, V., and Schmidt, F. Accurate in silico simulation of the rabbit purkinje fiber electrophysiological assay to facilitate early pharmaceutical cardiosafety assessment: Dream or reality? *Journal of Pharmacological and Toxicological Methods*, 115:107172, 2022.
- Nguyen, T. N. K., Dairay, T., Meunier, R., Millet, C., and Mougeot, M. Fixed-budget on-line adaptive learning for physics-informed neural networks. towards parameterized problem inference. In *International Conference on Computational Science*, pages 453–468. Springer, 2023.
- O’Leary, J., Paulson, J. A., and Mesbah, A. Stochastic physics-informed neural ordinary differential equations. *Journal of Computational Physics*, 468:111466, 2022.
- Raissi, M., Perdikaris, P., and Karniadakis, G. E. Physics-informed neural networks: A deep learning framework for solving forward and inverse problems involving nonlinear partial differential equations. *Journal of Computational physics*, 378:686–707, 2019.
- Sahli Costabal, F., Yang, Y., Perdikaris, P., Hurtado, D. E., and Kuhl, E. Physics-informed neural networks for cardiac activation mapping. *Frontiers in Physics*, 8:42, 2020.
- Trayanova, N. A., Lyon, A., Shade, J., and Heijman, J. Computational modeling of cardiac electrophysiology and arrhythmogenesis: toward clinical translation. *Physiological Reviews*, 104(3):1265–1333, 2024.
- Williams, G. and Mirams, G. R. A web portal for in-silico action potential predictions. *Journal of pharmacological and toxicological methods*, 75:10–16, 2015.
- Yazdani, A., Lu, L., Raissi, M., and Karniadakis, G. E. Systems biology informed deep learning for inferring parameters and hidden dynamics. *PLoS computational biology*, 16(11):e1007575, 2020.

A Full cardiac action potential model

This section completes Section 2, we give the full equation details for the 8 considered ionic channels in the CAP model. All constants involved in the following equations are listed on Table 3. In the following, we denote $\sigma(z)$ the sigmoid function

$$\begin{aligned} \sigma : \mathbb{R} &\rightarrow]0; 1[\\ z &\mapsto \sigma(z) = \frac{1}{1+e^{-z}}. \end{aligned}$$

To lighten the notation, the dependence on \mathbf{X} of the voltage function is omitted (*i.e.* $V(t)$ is written instead of $V(t, \mathbf{X})$).

A.1 Channel directly impacted by the drug characteristics

We first depict the equations for the four currents whose conductance depend on the IC50 value of the tested drug, *i.e.* currents for which the $k_j(\cdot, \cdot)$ function is not equal to 1 in Equation (2).

A.1.1 Fast sodium current $I_{\text{Na-F}}$

$$I_{\text{Na-F}}(t, \mathbf{X}) = G_{\text{Na-F}} \times \left(1 + \frac{D}{\text{IC50}_{\text{Na-F}}} \right)^{-1} \times g_{\text{Na-F}}(t) \times (V(t) - E_{\text{Na-F}}),$$

where

$$g_{\text{Na-F}}(t) = f_{\text{Na-F}}(t) \times h_{\text{Na-F}}(t)$$

with these two functions satisfying the following ODEs:

$$\begin{aligned} \frac{df_{\text{Na-F}}}{dt}(t) &= \frac{\sigma\left(\frac{V(t)+25}{5}\right) - f_{\text{Na-F}}(t)}{0.005}, \\ \frac{dh_{\text{Na-F}}}{dt}(t) &= \frac{\sigma\left(-\frac{V(t)+69}{3.96}\right) - h_{\text{Na-F}}(t)}{2}. \end{aligned}$$

A.1.2 L-type calcium current I_{Ca}

$$I_{\text{Ca}}(t, \mathbf{X}) = G_{\text{Ca}} \times \left(1 + \frac{D}{\text{IC50}_{\text{Ca}}} \right)^{-1} \times g_{\text{Ca}}(t) \times (V(t) - E_{\text{Ca}}),$$

where

$$g_{\text{Ca}}(t) = f_{\text{Ca}}(t) \times h_{\text{Ca}}(t)$$

with these two functions satisfying the following ODEs:

$$\begin{aligned} \frac{df_{\text{Ca}}}{dt}(t) &= \frac{\sigma\left(\frac{V(t)+14.6}{5.5}\right) - f_{\text{Ca}}(t)}{0.7}, \\ \frac{dh_{\text{Ca}}}{dt}(t) &= \left(0.7e^{-0.0337 \times (V(t)+14.5)^2} + 0.04 \right) \times \frac{\sigma\left(-\frac{V(t)+31}{5.54}\right) - h_{\text{Ca}}(t)}{25.1}. \end{aligned}$$

A.1.3 Fast transient outward potassium current $I_{\text{TO-F}}$

$$I_{\text{TO-F}}(t, \mathbf{X}) = G_{\text{TO-F}} \times \left(1 + \frac{D}{\text{IC50}_{\text{TO-F}}} \right)^{-1} \times g_{\text{TO-F}}(t) \times (V(t) - E_{\text{K}}),$$

where

$$g_{\text{TO-F}}(t) = f_{\text{TO-F}}(t) \times h_{\text{TO-F}}(t)$$

with these two functions satisfying the following ODEs:

$$\begin{aligned}\frac{df_{\text{TO-F}}}{dt}(t) &= \frac{\sigma\left(\frac{V(t)+3}{15}\right) - r_{\text{TO-F}}(t)}{3.5 \times e^{-\frac{V^2}{900}} + 1.5}, \\ \frac{dh_{\text{TO-F}}}{dt}(t) &= \frac{\sigma\left(-\frac{V(t)+33.5}{10}\right) - s_{\text{TO-F}}(t)}{20 \times \left(\sigma\left(-\frac{V(t)+33.5}{10}\right) + 1\right)}.\end{aligned}$$

A.1.4 Rapidly activating delayed rectifier potassium $I_{\text{K-R}}$

$$I_{\text{K-R}}(t, \mathbf{X}) = G_{\text{K-R}} \times \left(1 + \frac{D}{\text{IC50}_{\text{K-R}}}\right)^{-1} \times g_{\text{K-R}}(t) \times (V(t) - E_{\text{K}}),$$

where

$$g_{\text{K-R}}(t) = f_{\text{K-R}}(t) \times \sigma\left(-\frac{V + 33}{22.4}\right)$$

with the function $f_{\text{K-R}}$ satisfying the following ODE:

$$\begin{aligned}\frac{df_{\text{K-R}}}{dt}(t) &= \left(\frac{0.00138 \times (V(t) + 7)}{1 - e^{-0.123 \times (V(t) + 7)}} - \frac{0.00061 \times (V(t) + 10)}{1 + e^{0.145 \times (V(t) + 10)}}\right) \\ &\quad \times \left(\sigma\left(\frac{V(t) + 50}{7.5}\right) - f_{\text{K-R}}(t)\right).\end{aligned}$$

A.2 Channel indirectly impacted by the drug

A.2.1 Late sodium current $I_{\text{Na-L}}$

$$I_{\text{Na-L}}(t, \mathbf{X}) = G_{\text{Na-L}} \times g_{\text{Na-L}}(t) \times (V(t) - E_{\text{Na-L}}),$$

where

$$g_{\text{Na-L}}(t) = f_{\text{Na-L}}(t) \times h_{\text{Na-L}}(t)$$

with these two functions satisfying the following ODEs:

$$\begin{aligned}\frac{df_{\text{Na-L}}}{dt}(t) &= \frac{\sigma\left(\frac{V(t)+30}{5}\right) - f_{\text{Na-L}}(t)}{15}, \\ \frac{dh_{\text{Na-L}}}{dt}(t) &= \frac{\sigma\left(-\frac{V(t)+75.6}{6.3}\right) - h_{\text{Na-L}}(t)}{120 + e^{\frac{V(t)+100}{25}}}.\end{aligned}$$

A.2.2 Sustained transient outward potassium current $I_{\text{TO-S}}$

$$I_{\text{TO-S}}(t, \mathbf{X}) = \mathbf{G}_{\text{TO-S}} \times g_{\text{TO-S}}(t) \times (V(t) - E_K),$$

where

$$g_{\text{TO-S}}(t) = f_{\text{TO-S}}(t) \times \left(h_{\text{TO-S}}(t) + \frac{1}{2} \sigma \left(-\frac{V + 33.5}{10} \right) \right)$$

with these two functions satisfying the following ODEs:

$$\begin{aligned} \frac{df_{\text{TO-S}}}{dt}(t) &= \frac{\sigma \left(\frac{V(t)+3}{15} \right) - f_{\text{TO-S}}(t)}{9 \times \sigma \left(-\frac{V(t)+3}{15} \right) + 0.5}, \\ \frac{dh_{\text{TO-S}}}{dt}(t) &= \frac{\sigma \left(-\frac{V(t)+33.5}{10} \right) - h_{\text{TO-S}}(t)}{3000 \times \sigma \left(-\frac{V(t)+60}{10} \right) + 30}. \end{aligned}$$

A.2.3 Slowly activating delayed rectifier potassium Current $I_{\text{K-L}}$

$$I_{\text{K-L}}(t, \mathbf{X}) = \mathbf{G}_{\text{K-L}} \times g_{\text{K-L}}(t) \times (V(t) - E_K),$$

where

$$g_{\text{K-L}}(t) = f_{\text{K-L}}(t) \times h_{\text{K-L}}(t)$$

with these two functions satisfying the following ODEs

$$\begin{aligned} \frac{df_{\text{K-L}}}{dt}(t) &= \left(\frac{7.19 \cdot 10^{-5} \times (V + 30)}{1 - \exp(-0.148 \cdot (V + 30))} + \frac{1.31 \cdot 10^{-4} \times (V + 30)}{\exp(0.0687 \cdot (V + 30)) - 1} \right) \\ &\quad \times \left(\sigma \left(\frac{V(t) - 1.5}{16.7} \right) - f_{\text{K-L}}(t) \right), \\ \frac{dh_{\text{K-L}}}{dt}(t) &= \frac{1}{4} \times \left(\frac{7.19 \cdot 10^{-5} \times (V + 30)}{1 - \exp(-0.148 \cdot (V + 30))} + \frac{1.31 \cdot 10^{-4} \times (V + 30)}{\exp(0.0687 \cdot (V + 30)) - 1} \right) \\ &\quad \times \left(\sigma \left(\frac{V(t) - 1.5}{16.7} \right) - h_{\text{K-L}}(t) \right). \end{aligned}$$

A.2.4 Inward rectifier current $I_{\text{K-I}}$

$$I_{\text{K-I}}(t, \mathbf{X}) = \mathbf{G}_{\text{K-I}} \times \left(1 + \frac{D}{\text{IC50}_{\text{K-I}}} \right)^{-1} \times g_{\text{K-I}}(t) \times (V(t) - E_K),$$

where

$$g_{\text{K-I}}(t) = \sigma \left(-\frac{V(t) + 92}{10} \right).$$

Constant	Value	Units
E_{Ca}	40	mV
E_{Na}	74	mV
E_K	-85	mV
G_{Ca}	0.078	nS
G_{NaI}	0.03	nS
G_{Na-F}	16.52	nS
G_{Kr}	0.03	nS
G_{Ks}	0.1505	nS
G_{K1}	0.29	nS
G_{TO-F}	0.06	nS
G_{TO-S}	0.02	nS

Table 3: Constant values for the ionic currents models.

B ODE Weights w^{ODE} Initialization Method

Several methods exist for initializing weights in neural networks. To effectively balance the contributions of each ODE in the loss function, we implement a specific weighting scheme. This method ensures that each ODE contributes proportionately to the ODE loss, facilitating stable and efficient training. Below is a step-by-step description of the method used:

- **Initial Weight Setting:** Begin by setting all weights to one. This provides a uniform starting point for the weight adjustment process.
- **Calculate initial ODE loss:** The network is run for a single forward pass, and the initial ODE loss is computed. This is done by calculating the loss after zero epochs.
- **Adjust weights for balance:** Adjust the weights such that the contributions from each ODE to the total loss are of the same order of magnitude.

Our system consists of 14 ODEs, each contributing differently to the ODE loss due to the inherent differences in their dynamics and scales. Using the method described above, that aims to address these disparities, the value of w^{ODE} found vary significantly in a range of 0.01 and 10,000. Without such weighting, certain ODEs with naturally larger magnitudes could dominate the loss, leading to suboptimal training and convergence. The chosen weights reflect the relative importance and scale of each ODE in the system. By balancing the contributions of each ODE, the training process becomes more stable and efficient. This balance ensures that the optimization algorithm does not focus disproportionately on any single ODE, leading to more uniform updates across the entire system.